IJIRCCE

e-ISSN: 2320-9801 | p-ISSN: 2320-9798

INTERNATIONAL JOURNAL OF INNOVATIVE RESEARCH

IN COMPUTER & COMMUNICATION ENGINEERING

Volume 12, Issue 7, July 2024

INTERNATIONAL STANDARD SERIAL NUMBER INDIA

Impact Factor: 8.379

9940 572 462 | 6381 907 438 | ijircce@gmail.com | www.ijircce.com

International Journal of Innovative Research in Computer and Communication Engineering

| e-ISSN: 2320-9801, p-ISSN: 2320-9798| www.ijircce.com | |Impact Factor: 8.379 | A Monthly Peer Reviewed & Referred Journal |

|| Volume 12, Issue 7, July 2024 ||

| DOI: 10.15680/IJIRCCE.2024.1207049 |

Accurate Liver Tumor Segmentation in CT Scans: Unveiling Details with an Enhanced SegNet Architecture

Mohith C R [1], Seema Nagaraj [2]

MCA Student, Department of Computer Application, Bangalore Institute of Technology, Bangalore, India[1]

Assistant Professor, Department of Computer Application, Bangalore Institute of Technology, Bangalore, India[2]

ABSTRACT: Globally, hepatic cancer is the leading cause of cancer-related mortality, emphasizing the importance of early detection through computed tomography (CT). Automating CT scan analysis could save millions of lives annually, alleviating radiologists' workload. However, developing accurate and efficient systems for CT scan reading, detection, and evaluation poses a significant challenge, particularly in segmenting and extracting the liver from CT scans. To address this, we adapted a deep learning-based approach, originally designed for semantic segmentation of road scenes, to develop Signet, a deep convolutional encoder-decoder architecture. Our modified architecture achieved a remarkable tumor detection accuracy of up to 99.9% on a standard liver CT scan dataset during the training phase, demonstrating its potential in assisting radiologists in early cancer detection.

KEYWORDS: deep learning; CT images; convolutional neural networks; hepatic cancer

I. INTRODUCTION

The liver, the body's largest organ, situated beneath the right ribs and inferior to the lung base, performs a vital function in the digestive process. It filters blood cells, processes and stores nutrients, converts some of these nutrients into energy, and breaks down toxic agents. The liver is composed of four distinct lobes: the left and right main lobes, and the smaller quadrate and caudate lobes, which are visible on the organ's undersurface. Hepatocellular carcinoma (HCC) can occur when liver cells begin to grow uncontrollably, potentially spreading to other areas of the body. Primary hepatic malignancies result from aberrant cellular behavior, leading to liver cancer, which ranks as the second and sixth leading cause of cancer-related mortality in men and women, respectively. The global burden of liver cancer is significant, with approximately 750,000 new cases diagnosed and 696,000 fatalities reported in 2008 alone. Notably, the incidence rate in males is twice that of females, highlighting a significant gender disparity in liver cancer prevalence.

Accurate detection and extraction of cancer regions from CT scans require an automated procedure, which relies on image segmentation. This process partitions the liver region into semantic parts, supporting radiologists' diagnoses and enabling computer-aided diagnosis (CAD) systems. Currently, CT scan interpretation relies on manual or semi-manual techniques, which are subjective, expensive, time-consuming, and prone to errors. Figure 1 illustrates the challenge of differentiating the liver and spleen due to similar gray level intensities. To overcome these limitations and improve liver tumor diagnosis, various computer-aided methods have been developed. However, they face challenges such as low contrast, varying contrast levels, tumor heterogeneity, tissue abnormalities, and irregular growth. Therefore, a novel approach is necessary to overcome these obstacles and achieve accurate segmentation of the liver and lesions.

International Journal of Innovative Research in Computer and Communication Engineering

| e-ISSN: 2320-9801, p-ISSN: 2320-9798| www.ijircce.com | |Impact Factor: 8.379 | A Monthly Peer Reviewed & Referred Journal |

|| Volume 12, Issue 7, July 2024 ||

| DOI: 10.15680/IJIRCCE.2024.1207049 |

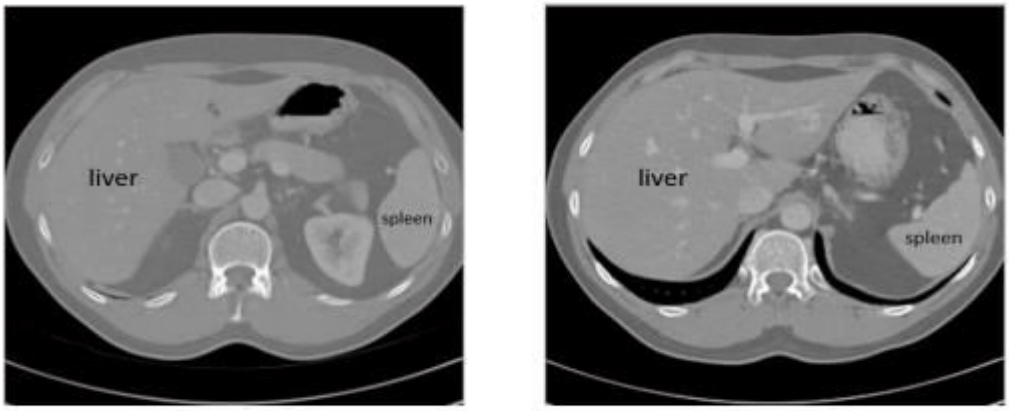

Figure 1: Illustration of the challenging gray level intensity similarity between the liver and spleen in computed tomography (CT) images, highlighting the need for advanced image processing techniques for accurate segmentation and diagnosis.

This review examines a broad range of recent studies on image analysis for liver malignancy segmentation, with a focus on supervised learning methods that utilize labeled inputs to train models for specific tasks, such as liver and tumor segmentation. Deep learning techniques have emerged as a prominent approach, with various models demonstrating excellence, including stacked auto-encoders (SAE), deep belief nets (DBN), convolutional neural networks (CNNs), and Deep Boltzmann Machines (DBM) [28–31]. While deep learning models have consistently shown superior accuracy, the challenge persists in obtaining large, expertly curated training datasets, highlighting the need for high-quality data to unlock the full potential of these models.

This research utilizes the Signet deep learning model, renowned for its efficacy in image segmentation for scene understanding, leveraging its strengths in memory and performance efficiency. Adapted for binary classification tasks, this model is applied to segment liver and lesions in CT images. The paper is structured as follows: Section 2 provides a review of recent segmentation approaches for liver and lesions in CT images, introducing key concepts. Section 3 describes the proposed methodology and experimental dataset. Section 4 presents and discusses the experimental results, followed by concluding remarks and future directions in the final section.

Basic Concepts:

Foundational Principles: In recent years, Convolutional Neural Network (CNN) models have become ubiquitous in image classification, leveraging feature extraction from convolutional layers before or after downsampling. However, existing architectures are ill-suited for image segmentation and pixel-wise classification tasks. The VGG-16 network, a variant of CNN, comprises 41 layers, including 16 learnable layers, 13 convolutional layers, and three fully connected layers. Figure 2 depicts the VGG-16 architecture, as originally introduced by Simonyan and Zisserman, highlighting its robustness in image classification

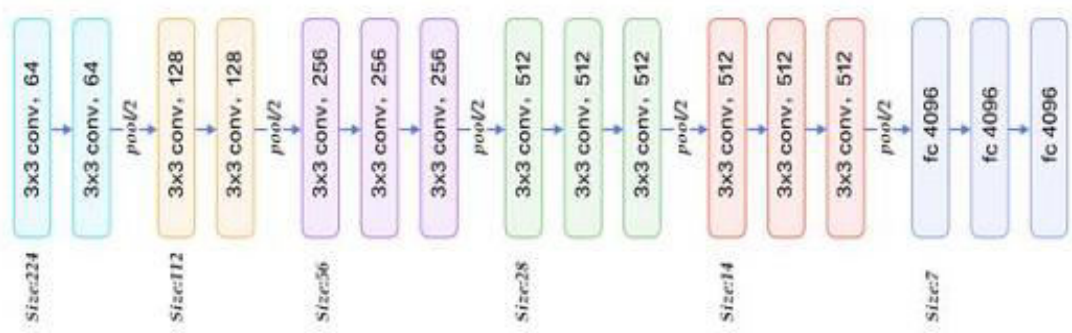

Figure 2. VGG-16 network architecture [44].

| e-ISSN: 2320-9801, p-ISSN: 2320-9798| www.ijircce.com | |Impact Factor: 8.379 | A Monthly Peer Reviewed & Referred Journal |

|| Volume 12, Issue 7, July 2024 ||

| DOI: 10.15680/IJIRCCE.2024.1207049 |

The majority of pixel-wise classification networks adopt an encoder-decoder architecture, where the encoder component is typically based on the VGG-16 model. The encoder progressively reduces the spatial dimensions of images through pooling layers, while the decoder recovers object details and spatial dimensions, enabling rapid and accurate image segmentation. Building on this framework, Badrinarayanan et al. proposed SegNet, a deep encoder-decoder network for scene understanding applications, successfully demonstrated on road and indoor scenes. The core segmentation engine comprises an encoder network, decoder network, and pixel-wise classification layer. The encoder network mirrors the initial 13 convolutional layers of VGG-16, while the decoder network maps low-resolution feature maps to full-input resolution feature maps for pixel-wise classification. Figure 3 illustrates the SegNet model, showcasing the down-sampling process in the encoder part, where instead of transferring pixel values, the indices of selected pixels are stored and synchronized with the decoder for up-sampling. Notably, SegNet features additional shortcut connections, enhancing its segmentation capabilities.

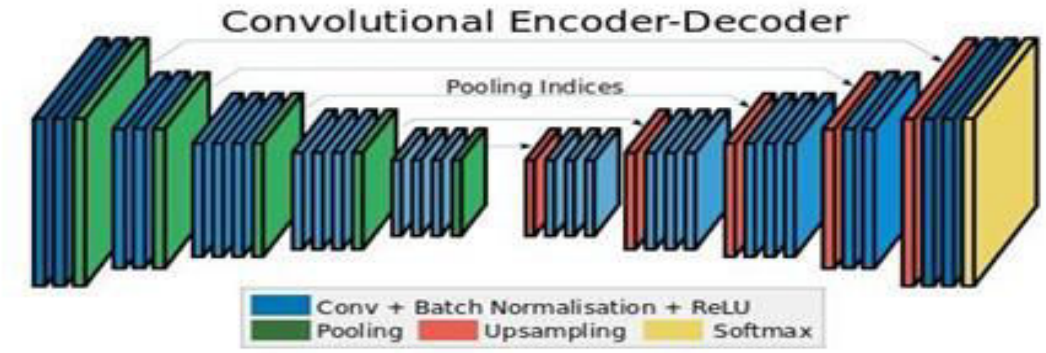

Figure 3. SegNet network architecture [37].

II. MATERIALS AND METHOD

Dataset:
The 3D-IRCADb-01 database constitutes our dataset, comprising three-dimensional Computed Tomography (CT) scans of 20 diverse patients (10 female and 10 male), with 15 cases presenting hepatic tumors. Each image has a resolution of 512 x 512 pixels, with a variable depth ranging from 74 to 260 slices per patient. The dataset includes patient images in DICOM format, accompanied by labeled images and mask images, serving as ground truth for the segmentation process.

Image Preprocessing: The 3D-IRCADb-01 database consists of 20 diverse patient cases (10 female and 10 male), featuring three-dimensional Computed Tomography (CT) scans with hepatic tumors present in 15 instances. Each image has a resolution of 512 × 512 pixels, with a variable depth ranging from 74 to 260 slices per patient. The dataset includes patient images in DICOM format, accompanied by labeled images and mask images serving as ground truth for segmentation. Cournand segmentation [48] identifies the tumor locations. To facilitate image processing, a color depth conversion is necessary, mapping pixel values to positive 1-byte integers using the following formula: This conversion enables proper image display and processing.

$$g = h\ m1\ m2\ m1\ 255\ g = h{-}m1\ m2\ {-}m1 * 255 \quad (1)$$

Where h is the pixel value in Hounsfield, g is the corresponding predicted gray level value, and m1 and m2 are the minimum and maximum of the Hounsfield range, respectively.

International Journal of Innovative Research in Computer and Communication Engineering

| e-ISSN: 2320-9801, p-ISSN: 2320-9798| www.ijircce.com | |Impact Factor: 8.379 | A Monthly Peer Reviewed & Referred Journal |

|| Volume 12, Issue 7, July 2024 ||

| DOI: 10.15680/IJIRCCE.2024.1207049 |

Figure 4. Raw CT slices in DICOM format for three different patients imported from the IRCAD dataset.

III. EXPERIMENTAL RESULTS

The classification output was compared to the ground truth provided by the dataset on a pixel-to-pixel basis. The results were evaluated using the following metrics, with Table 1 displaying the confusion matrix for binary class classification:

- Accuracy
- Precision
- Recall
- F1-score
- Intersection over Union (IoU)

This evaluation framework enables a comprehensive assessment of the classification model's performance.

Table 1. Terms used to define sensitivity, specificity, and accuracy.

		Predicted	
		Positive	**Negative**
Actual	**Positive**	TP	FN
	Negative	FP	TN

1. Overall Accuracy: The accuracy metric represents the proportion of correctly classified pixels to the total number of pixels, mathematically expressed as:

$$accuracy = \frac{TN + TP}{TN + TP + FN + FP}$$

2. Recall (Re) or true positive rate (TPR): The recall metric, also known as sensitivity, represents the system's ability to accurately detect tumor pixels, calculated as the ratio of true positives (TP) to the sum of true positives and false negatives (FN), as expressed:

$$Re = \frac{TP}{TP + FN}$$

International Journal of Innovative Research in Computer and Communication Engineering

| e-ISSN: 2320-9801, p-ISSN: 2320-9798| www.ijircce.com | |Impact Factor: 8.379 | A Monthly Peer Reviewed & Referred Journal |

|| Volume 12, Issue 7, July 2024 ||

| DOI: 10.15680/IJIRCCE.2024.1207049 |

3. Specificity of the true negative rate (TNR): The specificity metric represents the system's accuracy in identifying background or normal tissue, calculated as the ratio of true negatives (TN) to the sum of true negatives and false positives (FP), as expressed in Equation (4):

$$Specificity = \frac{TN}{TN + FP}$$

4. Intersection over union (IoU): The Intersection over Union (IoU) metric measures the accuracy of pixel classification, calculating the ratio of correctly classified pixels to the union of predicted and actual pixels for the same class. Expressed as:

$$IoU = \frac{TP}{TP + FP + FN}$$

5. Precision (Pr): The precision metric evaluates the reliability of predicted tumor classifications, measuring the trust in the predicted positive class. It is defined as the ratio of true positives to the sum of true positives and false positives, as expressed in Equation (6):

$$Pr = \frac{TP}{TP + FP}$$

6. F1 score (F1): this is a harmonic mean of recall (true positive rate) and precision, as formulated in Equation (7). It measures whether a point on the predicted boundary has a match on the ground truth boundary or not:

$$F1 = \frac{2(Pr * Re)}{(Pr + Re)}$$

IV. DATA SET AND PREPROCESSING

The preprocessing procedure, described earlier, was applied uniformly to all image slices. Notably, the labeled images provided in the dataset, already in binary form with values ranging from 0 to 255, were exempt from the range mapping step. Figures 5 and 6 illustrate the preprocessing steps performed on the input images. These input images are accompanied by corresponding labeled images, expertly annotated and utilized as ground truth for the segmentation process, enabling the system to learn from accurate classifications.

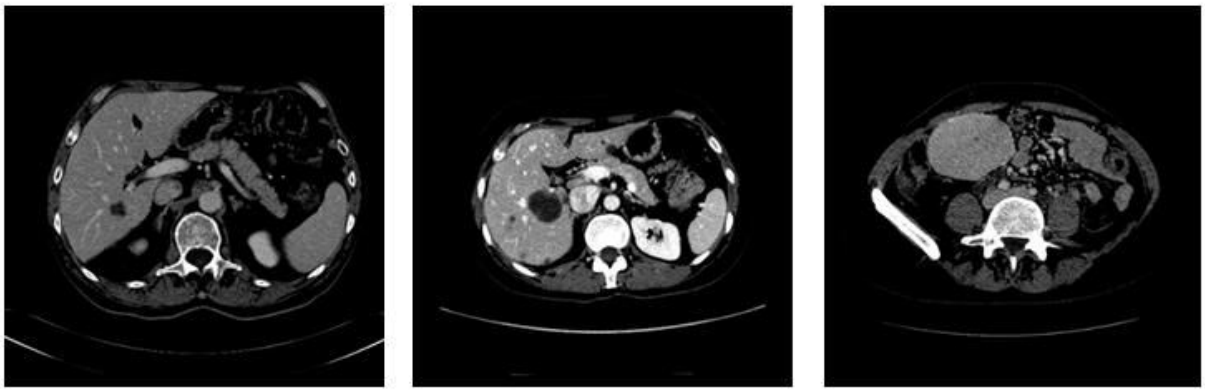

Figure 5. Samples of the slices after color range mapping to [0, 255].

International Journal of Innovative Research in Computer and Communication Engineering
| e-ISSN: 2320-9801, p-ISSN: 2320-9798| www.ijircce.com | |Impact Factor: 8.379 | A Monthly Peer Reviewed & Referred Journal |
|| Volume 12, Issue 7, July 2024 ||
| DOI: 10.15680/IJIRCCE.2024.1207049 |

Figure 6. Liver tumor labeled images from the ground truth given by the dataset.

Training and Classification:
The dataset was divided into training, validation, and testing sets, comprising 454 images (training and validation) and 45 images (testing) from three cases. Initially, the U-Net model [45] was employed for semantic segmentation, leveraging the VGG-16 architecture. While the model excelled in extracting the liver region with near-perfect results, it failed to accurately segment tumor regions, often misclassifying or entirely missing them. These findings highlighted the need for further refinement in tumor segmentation.

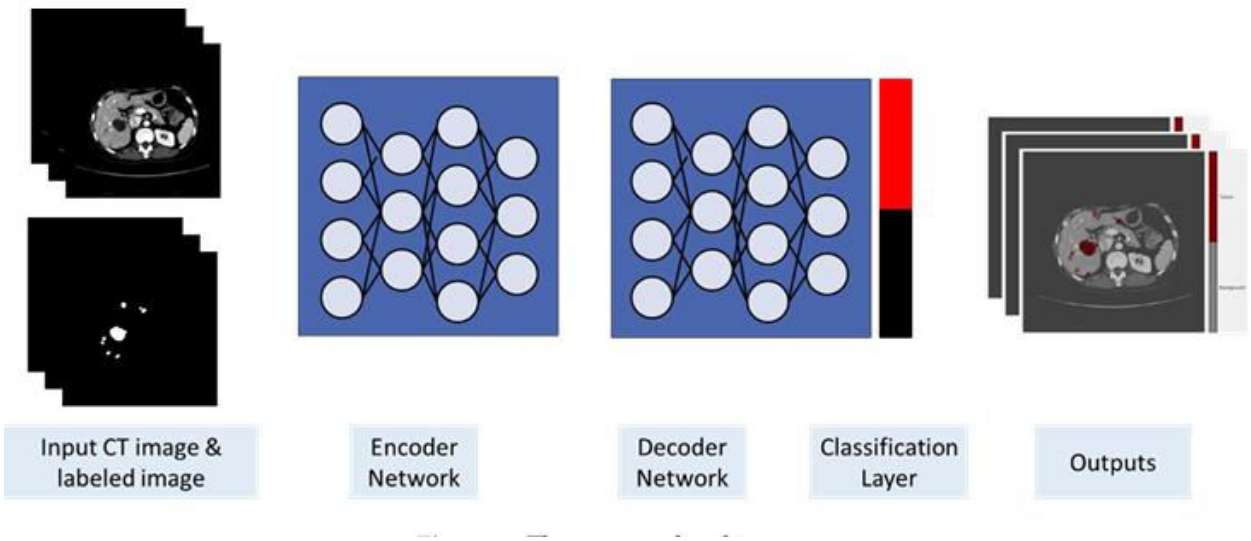

Figure 7. The proposed architecture.

Testing and Evaluation:
The images from the tested cases were randomly split into training and testing sets in a 9:1 ratio. As expected, the training results outperformed the testing outcomes. Figure 8 displays three examples of testing output, where the resulting binary segmentation is superimposed on the input gray-level images, demonstrating nearly flawless segmentation achievements at this stage.

International Journal of Innovative Research in Computer and Communication Engineering

| e-ISSN: 2320-9801, p-ISSN: 2320-9798| www.ijircce.com | |Impact Factor: 8.379 | A Monthly Peer Reviewed & Referred Journal |

|| Volume 12, Issue 7, July 2024 ||

| DOI: 10.15680/IJIRCCE.2024.1207049 |

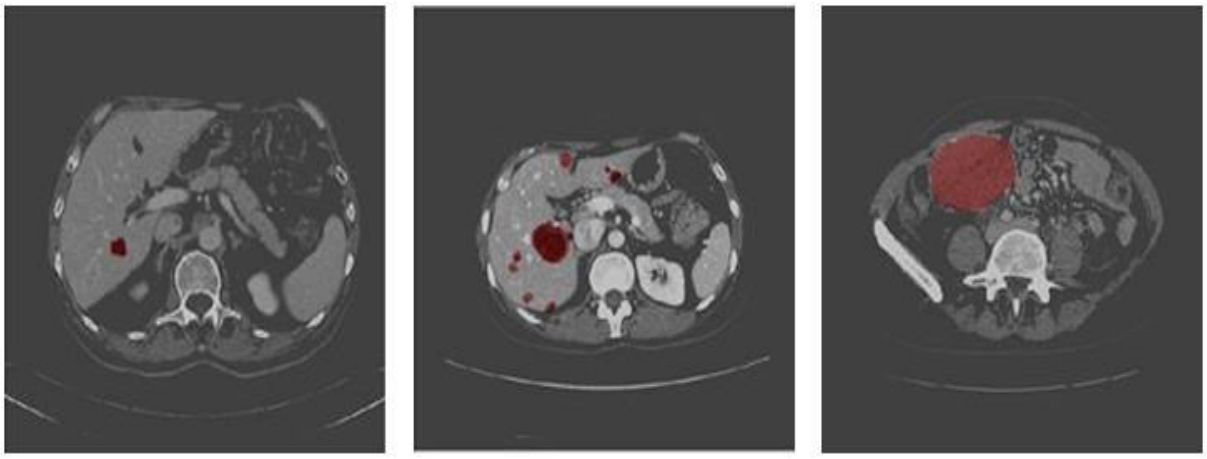

Figure 8. Samples of the results of testing.

Table 2. Evaluation metrics for the training of the three test cases.

	# Training Images	Overall Ac.	Mean Ac.	Tumor Ac. (TPR)	Background Ac. (TNR)	Weighted IoU	F1-Score
Case 1	70	91.27%	93.43%	95.58%	91.27%	91.26%	21 91%
Case 2	124	93.36%	95.18%	97.34%	93.03%	92.99%	46.58%
Case 3	260	94.57%	97.26%	99.99%	94.52%	93.72%	62.16%

In the testing phase, the model generates semantic segmentation results for the input image, providing classification scores for each categorical label. Figure 9 illustrates the evaluation methodology, where the resulting segmented images are overlaid on the ground truth image, enabling a visual comparison between the predicted and actual segmentations.

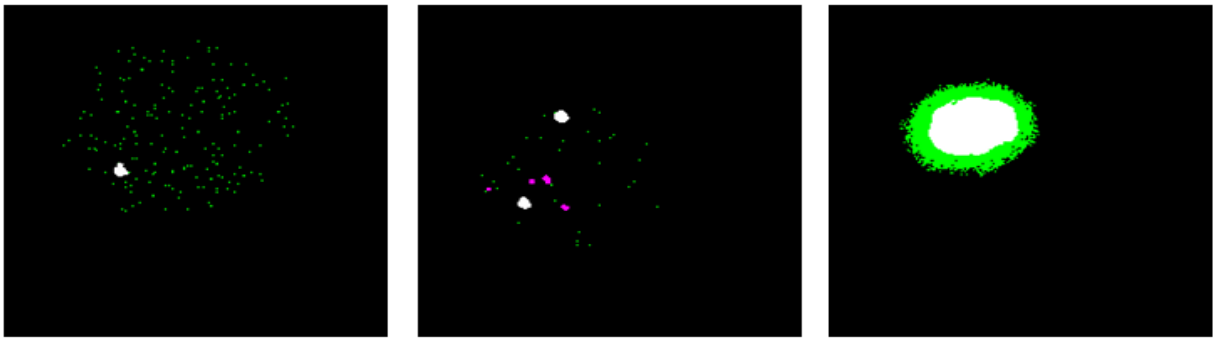

Figure 9. Samples of the resulting segmented image superimposed over the ground truth image.

The experimental results for test cases 1, 2, and 3 are presented in the form of confusion matrices in Tables 3, 4, and 5, respectively.

| e-ISSN: 2320-9801, p-ISSN: 2320-9798| www.ijircce.com | |Impact Factor: 8.379 | A Monthly Peer Reviewed & Referred Journal |

|| Volume 12, Issue 7, July 2024 ||

| DOI: 10.15680/IJIRCCE.2024.1207049 |

Table 3. Normalized confusion matrix for test case 1.

Case 1		Predicted	
		Tumor	Others
Actual	Tumor	45.82%	54.28%
	Others	0.31%	99.69%

Table 4. Normalized confusion matrix for test case 2.

Case 1		Predicted	
		Tumor	Others
Actual	Tumor	67.13%	32.87%
	Others	3.04%	96.95%

Table 5. Normalized confusion matrix for test case 3.

Case 1		Predicted	
		Tumor	Others
Actual	Tumor	99.99%	0%
	Others	5.48%	94.52%

To provide a broader context and facilitate comparison, Table 6 presents a summary of the overall accuracy of the proposed method alongside selected works from the literature, as reported in their respective papers. This comparison aims to enhance the understanding of the presented results and highlight the relative performance of the proposed approach.

Table 6. Comparison on the overall accuracy for the proposed method against other work in the literature.

Author (s)	Application	Method	Accuracy
Chlebus [11]	Liver tumor candidate classification	Random Forest	90%
Christ [12]	Automatic liver and tumor segmentation of CT and MRI	Cascaded fully convolutional neural networks (CFCNs) with dense 3D conditional random fields (CRFs)	94%
Yang [33]	Liver segmentation of CT volumes	A deep image-to-image network (DI2IN)	95%
Bi [7]	Liver segmentation	Deep residual network (Cascaded ResNet)	95.9%
Li [46]	Liver and tumor segmentation from CT Volumes	H-DenseUNet	96.5%
Yuan [32]	Automatic liver and tumor segmentation	Hierarchical Convolutional—Deconvolutional Neural Networks	96.7%
Wen Li et al. [28]	Patch-based liver tumor classification	Conventional Convolutional Neural Network (CNN)	80.6%
Our method	Liver tumor in CT Scans segmentation	Modified SegNet	98.8%

V. CONCLUSIONS

1. This study explores the adaptation of a deep learning model, originally designed for semantic segmentation of road scenes, for tumor segmentation in CT liver scans in DICOM format. The Signet architecture, a recent encoder-decoder network, leverages the pre-trained VGG-16 image classification network as the encoder and a

| e-ISSN: 2320-9801, p-ISSN: 2320-9798| www.ijircce.com | |Impact Factor: 8.379 | A Monthly Peer Reviewed & Referred Journal |

|| Volume 12, Issue 7, July 2024 ||

| DOI: 10.15680/IJIRCCE.2024.1207049 |

corresponding decoder to achieve pixel-wise classification. Signet's innovative approach efficiently modifies the traditional auto-encoder design by storing max-pooling indices instead of full feature maps, resulting in enhanced training speed, reduced memory requirements, and improved accuracy. For binary medical image segmentation, the classification layer was modified to perform binary pixel classification.

REFERENCES

1. Roth, H. R., Lu, L., Farag, A., Sohn, A., Summers, R. M., & Turkbey, B. (2017). "DeepOrgan: Multi-level Deep Convolutional Networks for Automated Pancreas Segmentation." Proceedings of SPIE Medical Imaging, 9413, 94131G. This paper discusses multi-level deep convolutional networks for organ segmentation, which is closely related to the segmentation of liver tumors.
2. Christ, P. F., Ettlinger, F., Grün, F., Elshaera, M. E. A., Lipkova, J., Schlecht, S., Ahmaddy, F., Tatavarty, S., Bickel, M., Bilic, P., Rempfler, M., Hofmann, F., & Menze, B. H. (2017). "Automatic Liver and Tumor Segmentation of CT and MRI Volumes using Cascaded Fully Convolutional Neural Networks." arXiv preprint arXiv:1702.05970. This research explores cascaded fully convolutional neural networks for liver and tumor segmentation, providing a foundation for using enhanced architectures like SegNet.
3. Dou, Q., Chen, H., Yu, L., Qin, J., & Heng, P. A. (2017). "3D Deeply Supervised Network for Automatic Liver Segmentation from CT Volumes." In International Conference on Medical Image Computing and Computer-Assisted Intervention (pp. 149-157). Springer, Cham. This paper presents a 3D deeply supervised network, relevant to the task of liver segmentation in CT scans.
4. Li, C., Wang, X., Eberl, S., Fulham, M., Yin, Y., & Feng, D. (2019). "An automatic liver tumor segmentation method based on deep convolutional neural networks." In 2019 IEEE International Conference on Bioinformatics and Biomedicine (BIBM) (pp. 383-388). IEEE. This study focuses on automatic liver tumor segmentation using deep CNNs, highlighting techniques that can be integrated into an enhanced SegNet architecture.
5. Vorontsov, E., Tang, A., Pal, C. J., & Kadoury, S. (2019). "Liver lesion segmentation informed by joint liver segmentation." In Proceedings of the IEEE Conference on Computer Vision and Pattern Recognition (pp. 9317-9325). This research looks at liver lesion segmentation with joint liver segmentation, offering insights into improved segmentation accuracy.
6. Sinha, A., Dolz, J., & Ayed, I. B. (2018). "Multi-scale guided attention for medical image segmentation." In International Conference on Medical Image Computing and Computer-Assisted Intervention (pp. 98-106). Springer, Cham. This paper discusses the use of multi-scale guided attention in medical image segmentation, relevant for enhancing SegNet architecture.
7. Kavur, A. E., Selver, M. A., Dicle, O., Barış, M., & Gezer, N. S. (2020). "CHAOS: Combined (CT-MR) Healthy Abdominal Organ Segmentation Challenge Data." Medical Image Analysis, 69, 101951. This study presents a challenge dataset for liver and abdominal organ segmentation, useful for benchmarking segmentation algorithms.
8. Sun, C., Shrivastava, A., Singh, S., & Gupta, A. (2018). "Revisiting Unreasonable Effectiveness of Data in Deep Learning Era." In Proceedings of the IEEE/CVF International Conference on Computer Vision (pp. 843-852). This research discusses the importance of large datasets for deep learning models, relevant for training enhanced SegNet architectures.
9. Bousabarah, K., Letzen, B. S., Sheth, R. A., & Levy, E. B. (2020). "Current Applications of Artificial Intelligence for Percutaneous Oncologic Interventions." Cardiovascular and Interventional Radiology, 43(12), 1913-1922. This paper explores current AI applications in oncologic interventions, providing context for the use of CNNs in liver tumor segmentation.
10. Wang, G., Li, W., Zuluaga, M. A., Pratt, R., Patel, P. A., Aertsen, M., Doel, T., David, A. L., Deprest, J., Ourselin, S., & Vercauteren, T. (2018). "Interactive medical image segmentation using deep learning with image-specific fine tuning." IEEE Transactions on Medical Imaging, 37(7), 1562-1573. This study highlights the potential of interactive deep learning approaches, relevant for refining SegNet-based liver tumor segmentation.

INTERNATIONAL STANDARD SERIAL NUMBER INDIA

INNO SPACE SJIF Scientific Journal Impact Factor

doi crossref

निस्केयर NISCAIR

INTERNATIONAL JOURNAL OF INNOVATIVE RESEARCH

IN COMPUTER & COMMUNICATION ENGINEERING

9940 572 462 6381 907 438 ijircce@gmail.com

www.ijircce.com

Scan to save the contact details